

Highly Stretchable, Low-Hysteresis, and Adhesive TA@MXene-Composited Organohydrogels for Durable Wearable Sensors

Ying Liu, Guoxing Tian, Yingjie Du, Pengju Shi, Na Li, Yunfeng Li, Zhihui Qin,*
Tifeng Jiao,* and Ximin He*

As wearable sensors advance rapidly, demands for multifunctional conductive soft materials are ever higher, including high stretchability, resilience, adhesiveness and stability, simultaneously in one material, for stable long-term use. Nanocomposite hydrogels incorporating conductive two-dimensional (2D) nanofillers, such as MXene-composited gels, emerge as promising candidates. Yet, fulfilling all above requirements, particularly large stretchability with low hysteresis, remains a challenge, owing to the easy oxidation and weak interactions of MXene nanosheets with polymer chains. Herein, an interfacial engineering strategy is proposed, where tannic acid (TA) with high-density hydroxyl groups is introduced to encapsulate MXene into a stable TA@MXene nano-motif and meanwhile increase the hydrogen-bonding interactions between TA@MXene and polymer network. By incorporating TA@MXene into poly(hydroxyethyl acrylate) (PHEA) network in a glycerol/water binary solvent, the obtained organohydrogel exhibits integrated properties of high stretchability (>500%) with low hysteresis (<3%), superior fatigue resistance (consistent hysteresis over 500 cycles at 300% strain), good adhesiveness, along with long-term stability (>7 days) and antifreezing abilities (−40 °C). Such organohydrogels demonstrate superior strain-sensitivity and thermosensitive capacities, enabling accurate and reliable detection of human movements, electrocardiogram signals, and body temperature. This general approach of stabilizing nanomaterials while effectively enhancing nanomaterial-polymer bonding is applicable for synthesizing diverse high-performance nanocomposited gels.

1. Introduction

There is a growing demand and expanding application scenarios for flexible electronics that can mimic the perception of human skin by transforming external stimuli into electrical signals. Researchers have been highly motivated to investigate conductive soft materials and design them for promising applications in the areas of soft robotics, personal healthcare monitoring, and electronic skins.^[1,2] However, many challenging requirements continue to restrict their presence in practical applications, including having high flexibility, mechanical robustness, long-term durability, and skin-like sensory capabilities. Recently, various conductive nanofillers including one-dimensional (1D) nanotubes or nanowires, 2D nanosheets, and three-dimensional (3D) nanoflowers or nanostars have been used to construct conductive composite materials.^[3] Among them, 2D nanosheets have high aspect ratio and surface area, which make 2D nanosheets-based composite materials exhibit high sensing sensitivity under the mechanical deformations.^[4] MXene, a newly developed 2D transition metal carbide and carbonitride, has attracted

great attention as a building block for next-generation wearable sensors owing to its excellent mechanical strength, high electrical conductivity, unique layered structure, abundant surface functional groups (OH, −F, −O, etc.), and hydrophilicity.^[5–8] A wide variety of MXene-based composites such as fibers, textiles, films, and papers have been fabricated by a variety of integration technologies including wet-spinning, spray-coating, dip-drying, and vacuum-assisted filtration for flexible wearable sensors.^[9–12] However, these MXene-based composites usually exhibited much higher rigidity and limited stretchability, resulting in poor compatibility with human skin.

Hydrogels featuring unique properties, such as tissue-like softness, stimuli-responsiveness, and biocompatibility, provide an ideal substrate platform for constructing wearable sensors. Conductive nanofillers such as CNTs, graphene, metal nanowires have been incorporated into hydrogel network to construct

Y. Liu, G. Tian, N. Li, Y. Li, Z. Qin, T. Jiao
State Key Laboratory of Metastable Materials Science and Technology
Hebei Key Laboratory of Applied Chemistry
Hebei Key Laboratory of Nanobiotechnology
Hebei Key Laboratory of Heavy Metal Deep-Remediation in Water and Resource Reuse
Yanshan University
Qinhuangdao 066004, China
E-mail: zhqin@ysu.edu.cn; tfjiao@ysu.edu.cn

Y. Du, P. Shi, X. He
Department of Materials Science and Engineering
University of California
Los Angeles, CA 90095, USA
E-mail: ximinhe@ucla.edu

 The ORCID identification number(s) for the author(s) of this article can be found under <https://doi.org/10.1002/adfm.202315813>

DOI: 10.1002/adfm.202315813

conductive nanocomposite hydrogels.^[3] However, the poor hydrophilicity and lack of functional groups of these conductive fillers make them easily aggregate in polymer matrix, deteriorating the mechanical performances and sensing ability. Recently, MXene nanosheets have been integrated into various polymer substrates to fabricate MXene-composited hydrogel sensors.^[13,14] Although the abundant hydrophilic functional groups on the surfaces of MXene enable excellent dispersibility and the formation of non-covalent interactions with hydrogel matrixes, MXene-composited single-networked hydrogels have low strength and insufficient toughness due to the weak interfacial interactions between MXene nanosheets and hydrogel matrices.^[13] Introducing a sacrificial noncovalent bond strategy can increase the tensile mechanical properties of MXene-composited hydrogels, demonstrating great promise for their practical use as flexible sensors.^[15] Moreover, in order to ensure long-term use in various environments, organic solvents such as ethylene glycol, dimethyl sulfoxide (DMSO), and glycerol (Gly), have been introduced in MXene-composited organohydrogel, endowing them with anti-freezing and anti-drying properties.^[16–20] Unfortunately, the high tensile properties in the hydrogels depend heavily on the mechanical energy dissipation from the sacrificial bonds, which require a long time to fully recover. Thus, highly stretchable and tough MXene-composited gels usually have high hysteresis and large residual strain, creating signal drift and response retardation in the flexible sensor's performance.^[21–24] Finally, MXene tends to oxidize in the presence of water and dissolved oxygen for prolonged periods of time, leading to a significant reduction in its conductivity and in its mechanical performance.^[25–31] As a result, the performance of MXene-composited gels deteriorates over time, making their long-term usage in wearable sensors less desirable.^[30,32] Therefore, it is necessary yet highly challenging to engineer MXene-based gels with the desired mechanical properties (high stretchability, toughness, and low hysteresis, etc.) and highly stable performance during the practical applications.

In this work, a MXene-composited organohydrogel of high and stable performance is prepared, by coating MXene nanosheet with tannic acid (TA) (TA@MXene nano-motif) and then introducing to physically crosslink poly(hydroxyethyl acrylate) (PHEA) network in a binary solvent of Gly/water environment (Figure 1a,d). Here, TA, a natural antioxidant containing a large number of hydrophobic aromatic rings and hydrophilic phenolic hydroxyl groups, is selected to encapsulate MXene nanosheets through hydrogen bonds, greatly improving their stability in aqueous solution. The introduced TA also generates plenty of hydrogen bond interactions with gel matrix. Specifically, the high density of hydrogen bonding between PHEA chains and TA@MXene provides a mechanism of energy dissipation and meanwhile limits the slippage between polymer chains, endowing the PHEA-TA@MXene organohydrogel with high stretchability, good toughness, and low hysteresis. More importantly, the Gly/water binary solvent and highly stable TA@MXene make PHEA-TA@MXene organohydrogel keep stable performance in long-term use and under extreme conditions. In addition, the organohydrogel exhibits suitable adhesion to common surfaces. Combining the superior mechanical properties with the conductivity and thermosensitive capabilities of MXene nanosheets, the organohydrogel exhibits high strain sensitivity with a broad working range, excellent stability, and superb thermosensitive

capacities. The resulting organohydrogel-based wearable sensor can accurately monitor various human activities, electromyography (EMG), electrocardiography (ECG) signals, and human body temperature. The TA@MXene nano-motif in this work can be also incorporated into other gel networks, providing new opportunities for the development of high-performance MXene-composited gels for flexible electronic devices.

2. Results and Discussion

2.1. Preparation and Long-Term Stability of TA@MXene Dispersion

The $Ti_3C_2T_x$ MXene studied in this work was synthesized from Ti_3AlC_2 through selective etching of the aluminum layer in HCl/LiF solution, which was subsequently exfoliated by ultrasound to obtain MXene nanosheets with only a few layers thick (Figure S1, Supporting Information).^[33] The X-ray diffraction (XRD) spectrum (Figure S2a, Supporting Information) shows that the peak of Al layers at 39° has been weakened and the (002) peak shifted from 9.6° to 5.9° after etching and exfoliating,^[34] confirming the successful synthesis of MXene nanosheets. The structure of well-exfoliated MXene nanosheets was characterized by scanning electron microscopy (SEM) (Figure S2b, Supporting Information), transmission electron microscopy (TEM) (Figure S2c, Supporting Information), and atomic force microscopy (AFM) (Figure S2d, Supporting Information), revealing an ultrathin and smooth 2D nanosheets morphology. The X-ray photoelectron spectroscopy (XPS) on MXene nanosheets shows the existence of Ti, C, O, and F elements, indicating that the $-O$, $-OH$, and $-F$ terminal groups were present on the surface (Figure S3, Supporting Information). Although these large numbers of hydrophilic terminal groups increase the dispersibility of MXene nanosheets, the propensity for oxidation in aqueous dispersions can still greatly compromise the resulting hydrogel's properties.^[35–37] In order to improve the dispersibility and stability of MXene, TA was added to the MXene dispersion. The catechol groups on TA interact with the surface pendant groups of MXene nanosheets through coordination or hydrogen bonds, which form a passivation layer on the surface of MXene, as shown in Figure 1a. The XRD patterns in Figure S4 (Supporting Information) show that the TA@MXene exhibited an obvious moved peak (002) compared to that of pristine MXene, demonstrating the successful intercalation of TA into the MXene nanosheets. To further study the interfacial bonding between TA and MXene, Fourier transform infrared spectroscopy (FTIR) was conducted (Figure S5, Supporting Information). Comparison between TA, MXene, and TA@MXene samples show that TA@MXene exhibited not only the absorption peaks of TA (855 , 1024 , 1451 , and 1605 cm^{-1} corresponding to the stretching vibration of substituted benzene ring aromatic compounds) but also the shift of the peak related to O-H stretching vibration (from 3604 to 3323 cm^{-1} for MXene), indicating the formation of hydrogen bonding between TA and MXene nanosheets.^[38,39] The micromorphologies of TA@MXene characterized by TEM and SEM show that TA@MXene exhibited a sheet-like structure with a smooth surface (Figure S6, Supporting Information).

In order to assess the protective effect of TA on MXene nanosheets for long-term stability in a water environment, both

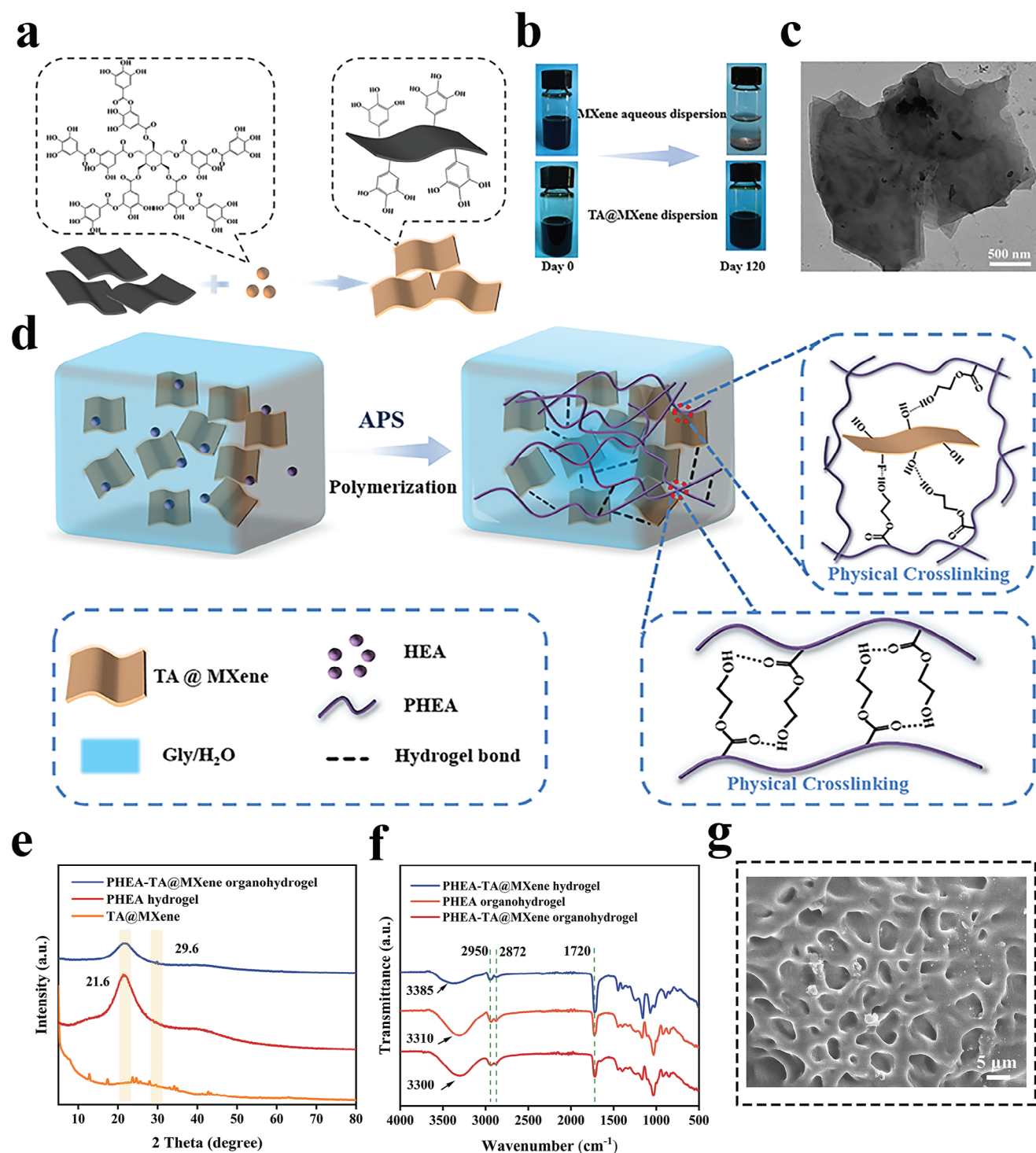


Figure 1. Preparation of TA@MXene dispersion and PHEA-TA@MXene organohydrogel. a) Schematic illustration of surface modification of MXene nanosheets with TA. b) Optical photographs of MXene aqueous dispersion and TA@MXene dispersion at 0 and 120 days. c) TEM image of TA@MXene reserved in aqueous solution after 120 days. d) Schematic illustration for the preparation of the PHEA-TA@MXene organohydrogel. e) XRD patterns of TA@MXene, PHEA hydrogel, and PHEA-TA@MXene organohydrogel. f) FTIR spectra of PHEA-organohydrogel, PHEA-TA@MXene hydrogel, and PHEA-TA@MXene organohydrogel. g) SEM image of the PHEA-TA@MXene organohydrogel.

TA@MXene and MXene colloidal dispersions were prepared and stored in open glass at room temperature. Photographs show that the as-prepared MXene dispersion presented a color change from dark green to gray and aggregated at the bottom of the bottle after being in storage for 120 days owing to the oxidation of MXene to TiO_2 .^[40,41] While TA@MXene dispersion maintained a dark green color without obvious aggregation similar to its initial state (Figure 1b). The micromorphologies of the stored MXene nanosheets were evaluated by TEM and SEM. The TEM image in Figure 1c shows that the TA@MXene preserved the nanosheet morphology with smooth surfaces after 120 days in aqueous solution. The SEM image of TA@MXene stored in water after 120 days showed similar nanosheet morphology (Figure S7, Supporting Information). These results show the effective protection of TA can provide for MXene nanosheets structure during the long-term storage. XPS was used to further analyze the oxidation degree and content changes of different elements of MXene nanosheets in MXene and TA@MXene aqueous dispersions. As expected, the presence of titanium (Ti), carbon (C), fluorine (F), and oxygen (O) in as-prepared and stored MXene were confirmed by the corresponding XPS spectra (Figures S3, S8, and S9, Supporting Information). High-resolution XPS spectra of MXene at varying storage conditions were fitted into Ti 2p, C 1s, and O 1s core levels (Figures S10 and S11, Supporting Information). The difference in TiO_2 content can be determined by the area statistics of Ti^{4+} valence peak of Ti in Ti 2p region (Figure S11, Supporting Information). The content of TiO_2 in the fresh MXene nanosheets was low (≈ 16.8 atom %). After MXene was stored in water for 120 days, the content of TiO_2 reached a high value of 93.2 atom %, while the content of TiO_2 in TA@MXene stored in aqueous solution for 120 days was only 5.2 atom %. Therefore, our results indicate that introducing TA is an effective way to retain the stability of MXene nanosheets in aqueous solutions.^[41,42] To summarize, the TA@MXene nano-motif designed in this work is highly stable in water environment, which is satisfactory for fabricating MXene-based gels for the long-term use.

2.2. Synthesis and Characterization of the PHEA-TA@MXene Organohydrogel

The PHEA-TA@MXene organohydrogel was prepared by incorporating the TA@MXene nano-motif into PHEA gel network in a Gly/water binary solvent, and the corresponding fabrication procedure is depicted in Figure 1d. The monomer 2-Hydroxyethyl acrylate (HEA) and solvent Gly were added into the TA@MXene aqueous dispersion under stirring to form a homogeneous solution. Then, the initiator ammonium persulfate (APS) was added into the mixed solution to induce the polymerization of HEA to obtain the PHEA-TA@MXene organohydrogel. The chain entanglements and hydrogen bonding between PHEA chains led to the hydrogen-bonded supramolecular networks, serving as the gel skeleton. TA@MXene nano-motif provided additional polyhydroxy groups that can form dense hydrogen bonds with PHEA chains, further contributing to the gel's mechanical strength and resilience. In addition, the presence of TA@MXene also endowed the organohydrogel with good conductivity and sensing capabilities. The introduced Gly encouraged more hydrogen bonding

within the crosslinked network, enhancing the ductility of the organohydrogel. It also formed strong hydrogen bond interactions with water,^[43] endowing the organohydrogel with excellent environmental stability.

Multiple characterizations were performed to compare the PHEA hydrogel, PHEA organohydrogel, PHEA-TA@MXene hydrogel, and PHEA-TA@MXene organohydrogel in order to better understand physicochemical structure of the PHEA-TA@MXene organohydrogel. The XRD spectrum of PHEA-TA@MXene organohydrogel exhibited a small peak at $2\theta = 29.6^\circ$ (008) corresponding to the peak of TA@MXene and an amorphous peak at $2\theta = 21.6^\circ$ similar to that of PHEA hydrogel (Figure 1e),^[42] indicating the successful binding and well dispersion of MXene nanosheets in the organohydrogel network. FTIR spectra were characterized to analyze the intermolecular interaction of PHEA-TA@MXene organohydrogel, as shown in Figure 1f. For all the prepared samples, the C=O stretching band located at 1720 cm^{-1} was observed. After adding Gly, the peak of -OH stretching vibration at 3385 cm^{-1} in PHEA-TA@MXene hydrogel transferred to 3300 cm^{-1} in PHEA-TA@MXene organohydrogel. Compared with the peak of -OH stretching vibration at 3310 cm^{-1} in PHEA organohydrogel, the corresponding peak of -OH stretching vibration shifted to 3300 cm^{-1} in PHEA-TA@MXene organohydrogel. These results demonstrate the formation of hydrogen bonding interactions between MXene nanosheets, Gly molecules and PHEA chains. The SEM image shows that the PHEA-TA@MXene organohydrogel had open pore architecture (Figure 1g), and the corresponding EDS elemental mapping images of C, O, F, and Ti elements in Figure S12 (Supporting Information) indicates that MXene nanosheets were distributed homogeneously in the gel matrix.

2.3. Mechanical Performances of the PHEA-TA@MXene Organohydrogel

The mechanical properties of the PHEA-TA@MXene organohydrogel were quantitatively evaluated by tensile test. The PHEA hydrogel had poor tensile properties with a tensile strain of 295% and a tensile strength of 33.6 kPa (Figure 2a). When TA@MXene was incorporated, the tensile strain and strength of the prepared PHEA-TA@MXene hydrogel increased by 49% and 132%, respectively. When Gly was introduced to create PHEA-TA@MXene organohydrogel, the tensile strain and strength reached to 690% and 85 kPa, increasing by 134% and 153% compared to that of the PHEA hydrogel, respectively, both of which were higher than that of PHEA-TA@MXene hydrogel. Moreover, the addition of TA@MXene greatly improved the elastic modulus and toughness of PHEA-TA@MXene hydrogel and organohydrogel (Figure S13, Supporting Information). The introduction of Gly substantially contributed to the increase of toughness but slightly decreased the elastic modulus. The PHEA-TA@MXene organohydrogel with skin-like elastic modulus (12.5 kPa) exhibited a high toughness of 276.3 kJ m^{-3} , superior to those of the PHEA (58.2 kJ m^{-3}) and PHEA-TA@MXene hydrogels (160.4 kJ m^{-3}). The greatly enhanced mechanical properties of the PHEA-TA@MXene organohydrogel may be ascribed to the increased crosslinking density and reduced interchain friction. TA@MXene as multifunctional crosslinkers

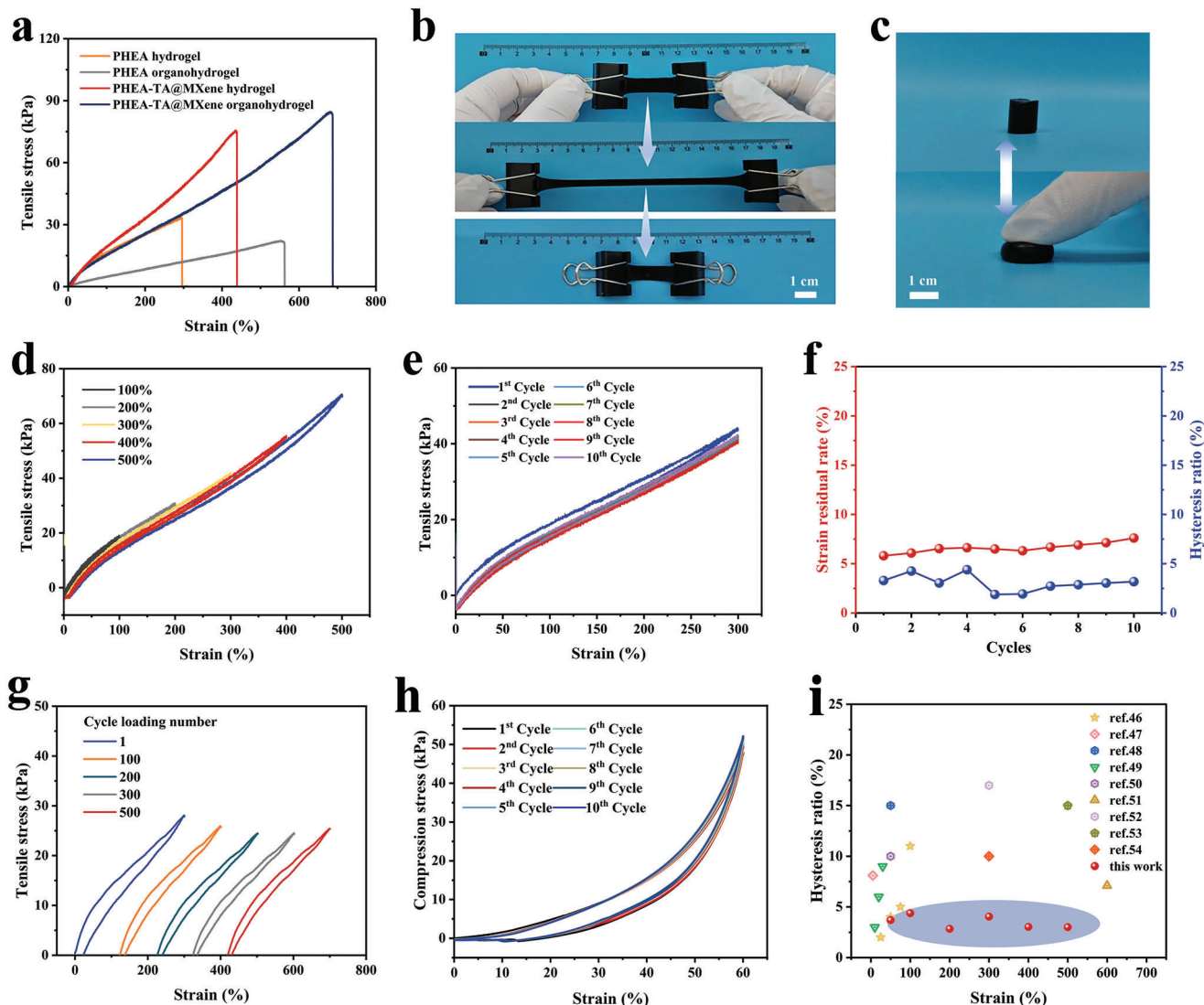


Figure 2. Mechanical properties of the PHEA-TA@MXene organohydrogel. a) Typical tensile stress-strain curves of the PHEA hydrogel, PHEA organohydrogel, PHEA-TA@MXene hydrogel, and PHEA-TA@MXene organohydrogel. Photos showing b) stretching and c) pressing process of the PHEA-TA@MXene organohydrogel. d) Tensile loading-unloading curves of PHEA-TA@MXene organohydrogel at varied strains (100, 200, 300, 400, and 500%). e) Ten successive loading-unloading cycles and f) the corresponding strain residual rate and hysteresis ratio of PHEA-TA@MXene organohydrogel at a strain value of 300%. g) Consecutive loading-unloading tensile cycles of PHEA-TA@MXene organohydrogel under 300% strain with the various cycles up to 500 and the curves are horizontally offset for clarity. h) Ten compression cycles of the PHEA-TA@MXene organohydrogel under 60% strain. i) Comparison of hysteresis and strain performances of our PHEA-TA@MXene organohydrogel with reported nanocomposite gels.

can form abundant hydrogen bonds with the PHEA chains owing to the polyhydroxy groups of TA, and meanwhile reduce the hydrogen bonds between polymer chains, contributing to the mobility of chains. The high-density hydrogen bonds can effectively handle higher loads and dissipate energy when these bonds are broken. This hypothesis is supported by the PHEA-MXene organohydrogel (without TA) showing relatively low tensile strain (465%), strength (66.1 kPa), and toughness (143.02 kJ m^{-3}) (Figure S14, Supporting Information). The incorporation of Gly can form weaker hydrogen bond crosslinking with polymer chains and decrease the hydrogen bonds between polymer chains, promoting the movement of polymer chains to resist a larger strain, which is verified by

the fact that the PHEA organohydrogel became more ductile (Figure 2a).

The effect of TA@MXene content on the mechanical performance of the PHEA-TA@MXene organohydrogel was explored (Figure S15, Supporting Information). Increasing TA@MXene content would gradually increase tensile strength and toughness of the PHEA-TA@MXene organohydrogel, while the tensile strain and elastic modulus initially increased but ultimately decreased. The increased TA@MXene improved the cross-linking density, but excessive amounts can lead to aggregation, reducing stretchability.^[44,45] The Gly content also has great influence on the mechanical performance of the organohydrogels (Figure S16, Supporting Information). Increasing the Gly content

increased tensile strength, stretchability and toughness, while the elastic modulus decreased. This suggests Gly can promote skin-like mechanical properties in PHEA-TA@MXene organohydrogels. Finally, having higher monomer concentration can improve the tensile strength and stiffness but will reduce the stretchability (Figure S17, Supporting Information).^[46] Based on the above analysis, PHEA-TA@MXene organohydrogels prepared with 30 wt.% HEA and 0.3 wt.% MXene in a 1:1 Gly/water binary solution provides a gel with the superior combination of the tensile strength (85 kPa), elastic modulus (12.5 kPa), stretchability (690%), and toughness (276.3 kJ m⁻³), which was used for subsequent experiments.

In addition to high stretchability and toughness, the PHEA-TA@MXene organohydrogel also exhibited high resilience and low hysteresis, which are vital qualities for flexible sensors. An organohydrogel rectangular strip (25 mm × 10 mm) can withstand large deformations of stretching and rapidly recover to its initial length after the external load was released (Figure 2b; and Movie S1, Supporting Information). Similarly, a columnar sample placed under compression forces can also deform under large loads and quickly bounce back during the release process (Figure 2c; and Movie S2, Supporting Information). Cyclic tensile tests were conducted to investigate the resilience and hysteresis behavior. Figure 2d shows the cyclic tensile curves of the PHEA-TA@MXene organohydrogel at different maximum strains (100–500%). For all loading-unloading cycles under different strains, very small hysteresis loops were observed. Although the amount of dissipated energy continued to increase with higher strain, the hysteresis maintained a value ≈5% across the different degrees of stretching (Figure S18, Supporting Information). These results demonstrate that the PHEA-TA@MXene hydrogel can dissipate more energy at large strains to endure the loading, and possesses high resilience after the unloading.^[22] Ten successive cyclic tensile experiments at a strain of 300% shows that the hysteresis loops of ten cycles approximately overlapped (Figure 2e). The residual strain and hysteresis of the PHEA-TA@MXene organohydrogel after ten successive tensile cycles were ≈6% and 4%, respectively (Figure 2f), demonstrating the excellent elasticity and quick self-recovery ability at large strain. Moreover, the hysteresis behavior of the PHEA-TA@MXene organohydrogel was almost independent of strain rates (Figure S19, Supporting Information).

The superior resilience and low hysteresis of the PHEA-TA@MXene organohydrogel may be attributed to the high-density hydrogen bonds between TA@MXene and PHEA chains. When loading, some hydrogen bonds between PHEA chains can be dissociated to promote the movement of polymer chains, contributing to the high stretchability. The high-density hydrogen bonds formed strong crosslinked interactions, which can provide the high elastic retraction to polymer chains, thus facilitating the rapid reassociation of the fractured hydrogen bonds after unloaded. This assumption is also verified by the phenomenon that the PHEA-TA@MXene hydrogel exhibited lower hysteresis while the PHEA organohydrogel without TA@MXene had the higher hysteresis (Figure S20, Supporting Information). To further test the fatigue hysteresis of the PHEA-TA@MXene organohydrogel, the successive 500 loading-unloading cycles of the same sample were conducted. As shown in Figure 2g, a nearly same hysteresis and negligible stress decline were observed after 500 cycles, indi-

cating the great cycling stability and excellent fatigue resistance of the PHEA-TA@MXene organohydrogel. Moreover, the successive ten cyclic compressive tests at a maximum strain of 60% in Figure 2h shows that the loading-unloading curve almost overlapped with each other, confirming the high resilience, and cycling stability again. In summary, compared with the previously reported nanocomposite gels, the PHEA-TA@MXene organohydrogel achieved the best combination of high stretchability and low hysteresis (Figure 2i).^[46–54]

2.4. Self-Adhesion of the PHEA-TA@MXene Organohydrogel

The PHEA-TA@MXene organohydrogel exhibited superb self-adhesive properties owing to the presence of catechol groups.^[14,33] As vividly displayed in Figure 3a, the cylindrical organohydrogel sample can adhere tightly to the surface of a variety of substrates, including polyvinyl chloride (PVC), polyethylene glycol terephthalate (PET), a copper sheet and a glass slide, and lift them up with ease. This demonstrates the outstanding adhesion strength on a broad range of substrates including rubber, metals, glass, and plastic materials. Subsequently, copper sheets, glass slides, PVC slides, PET plastics and filter paper were selected as representative substrates for the lap-shear test in tensile mode to quantitatively evaluate the adhesive strength of the PHEA-TA@MXene organohydrogel, which was recorded by maximal shear stress of the organohydrogel to different surfaces. Figure 3b shows the adhesion mechanical curves of the organohydrogel to different substrates at room temperature and the corresponding adhesive strength is displayed in Figure 3c. The organohydrogel exhibited moderate lap-shear stress and the corresponding adhesive strength to different substrates ranged from 4.6 to 27.2 kPa. Due to the nature of catechol groups, our material can be compatible with a wide range of materials and application scenarios that wearable sensors could potentially encounter.

2.5. Environmental Tolerance of the PHEA-TA@MXene Organohydrogel

Hydrogels face two major obstacles when it comes to long-term practical applications: water loss at room temperature and freezing at low temperature.^[18] The formation of Gly/water binary solvent in the PHEA-TA@MXene organohydrogel endowed it with excellent environmental stability such that it retained water and exhibited ant-freezing behavior significantly better than traditional hydrogels.^[55] The material's water retention capabilities was explored first. Figure 3d shows the morphological changes of PHEA-TA@MXene hydrogel and organohydrogel after being exposed to air for 7 days. The organohydrogel almost remained its initial shape and size, while the hydrogel shrank dramatically owing to water loss. In order to evaluate the effectiveness of Gly in improving the anti-dehydration ability of the organohydrogel, the weight changes of PHEA-TA@MXene hydrogel and organohydrogel were recorded at different storage times. As shown in Figure 3e, the organohydrogel could quickly reach equilibrium state after 2 days and retain up to 80 wt.% of its weight within

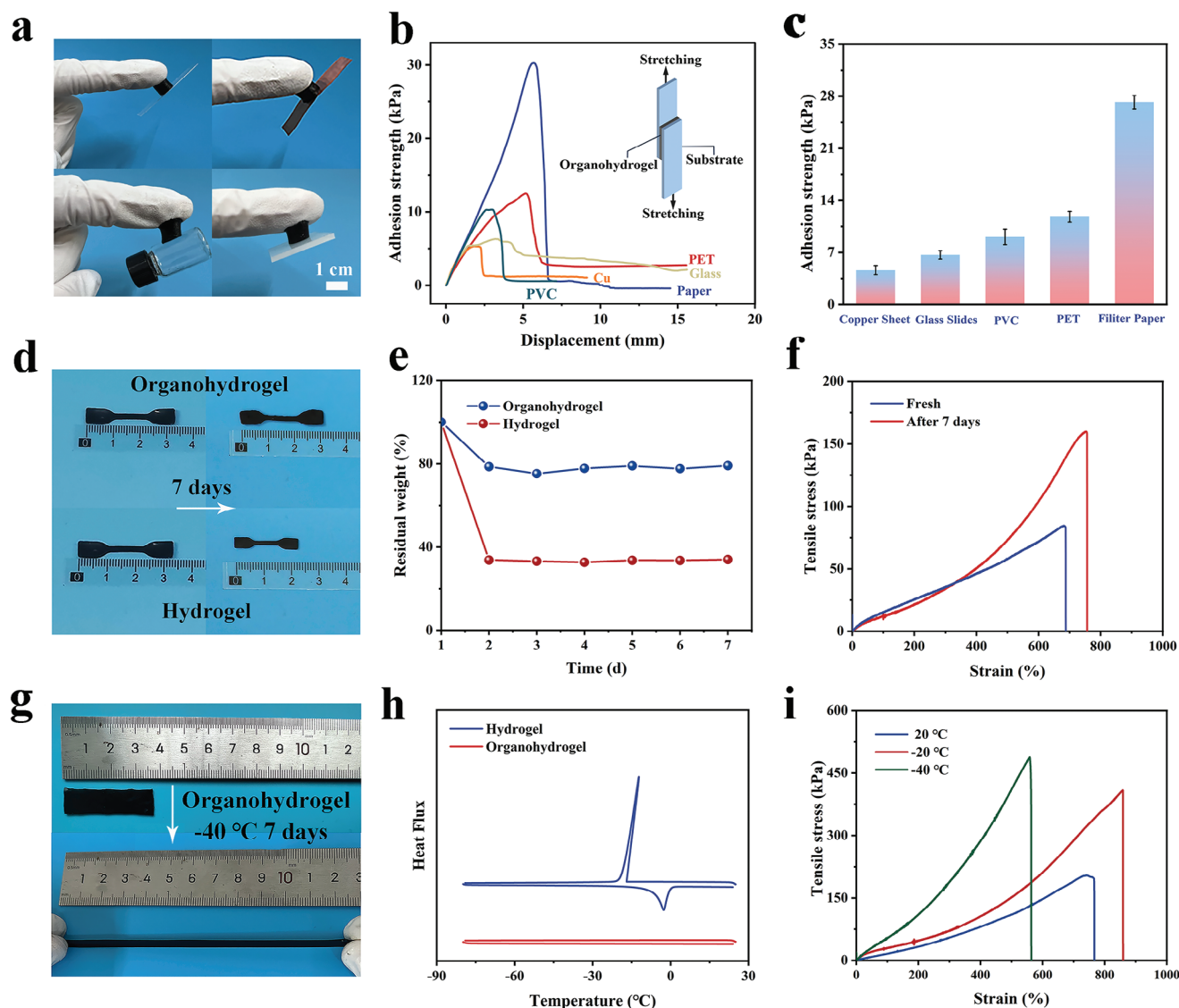


Figure 3. Adhesion properties and environmental tolerance of the PHEA-TA@MXene organohydrogel. a) Photographs illustrating the adhesiveness of the PHEA-TA@MXene organohydrogel to diverse surfaces, including copper sheet, PVC, PET, and glass. b) Adhesion mechanical curves (Inset: schematic illustration of the adhesion testing process) and c) adhesive strength of the PHEA-TA@MXene organohydrogel to various substrates. d) Optical images of the PHEA-TA@MXene hydrogel and organohydrogel after stored at room temperature for 7 days. e) Weight retaining of PHEA-TA@MXene organohydrogel and hydrogel after stored at room temperature within 7 days. f) Typical tensile stress-strain curves of PHEA-TA@MXene organohydrogel before and after stored at room temperature for 7 days. g) Digital images showing the stretching of the PHEA-TA@MXene organohydrogel after 7 days of freezing at $-40\text{ }^{\circ}\text{C}$. h) DSC curves of PHEA-TA@MXene hydrogel and organohydrogel. i) Typical tensile stress-strain curves of PHEA-TA@MXene organohydrogel at different temperatures (20, -20 , and $-40\text{ }^{\circ}\text{C}$).

7 days storage at ambient conditions (temperature: $25\text{ }^{\circ}\text{C}$, RH = 23%). In contrast, after 2 days of storage, the water in the hydrogel evaporated almost completely and only 30 wt.% of the initial weight was retained. Tensile tests indicate that the organohydrogel exhibited increased mechanical performances with a tensile strain of 780% and a tensile strength of 160 kPa after 7 days of storage (Figure 3f). This can be attributed to partial evaporation of water in the organohydrogel and a more condensed polymer network due to long-term exposure to air. Although a small change in mechanical performance for the organohydrogel after 7 days of stor-

age was observed compared to the as-prepared organohydrogel, the mechanical flexibility was still very desirable for practical applications.

The low freezing point of Gly/water binary solvent also endowed PHEA-TA@MXene organohydrogel with excellent anti-freezing properties. As shown in Figure 3g, after being stored at $-40\text{ }^{\circ}\text{C}$ for 7 days, the organohydrogel still had high flexibility to withstand large stretching. Differential scanning calorimetry (DSC) measurements were conducted to offer deeper insights into the anti-freezing characteristics of the PHEA-TA@MXene organohydrogel, and the result is displayed in Figure 3h. A

distinct exothermic peak located at $-16\text{ }^{\circ}\text{C}$ can be seen in the hydrogel, while no crystallization peak was observed within the temperature range of -80 to $25\text{ }^{\circ}\text{C}$ for the organohydrogel, indicating the introduction of Gly effectively inhibited the generation of ice crystals by forming hydrogen bonds with water molecules. Subsequently, the mechanical stability of the PHEA-TA@MXene organohydrogel at low temperature was evaluated by tensile tests (Figure 3i). When cooled from the room temperature to $-20\text{ }^{\circ}\text{C}$, both the tensile strain and strength of the PHEA-TA@MXene organohydrogel increased, reaching to 857% and 405 kPa, respectively. This change may be attributed to the enhanced hydrogen bonding interactions in the gel network.^[56] Even at $-40\text{ }^{\circ}\text{C}$, the PHEA-TA@MXene organohydrogel still had the high stretchability of 560%. Collectively, the PHEA-TA@MXene organohydrogel exhibited excellent environmental stability. Moreover, SD rats-skin-contact experiments were conducted to evaluate the biosafety of PHEA-TA@MXene organohydrogels. The back hair of SD rats was depilated, followed by the application of the PHEA-TA@MXene organohydrogel onto their dorsal integument. After one week, the part of the skin in contact with the organohydrogel sliced and stained with hematoxylin-eosin (H&E) for histological analysis. As shown in Figure S21 (Supporting Information), for organohydrogel group, the structural morphology of dermis and epidermis was normal and few inflammations were observed, which was similar to the negative control. These results indicate that the PHEA-TA@MXene organohydrogel exhibited good on-skin biosafety.

2.6. Application as Wearable Sensors

The incorporation of MXene provides the PHEA-TA@MXene organohydrogel with good electrical conductivity. When TA@MXene content increased from 0 to 0.4 wt.%, the conductivity of the PHEA-TA@MXene organohydrogel first increased and then slightly decreased (Figure S22, Supporting Information). This may be explained by that the transport and hopping of electrons in MXene nanosheets and the migration of free ions (such as hydrogen ions ionized from water, SO_4^{2-} from initiator APS) via free water contributed to the conductivity. The increase of MXene content increased the electron transport and hopping paths, thus enhancing electron conduction, but decreased the size of ion channels.^[57,43] The competition between increased electron conduction and decreased ion conduction influenced the variation of conductivity. The conductivity of the PHEA-TA@MXene organohydrogel was demonstrated by fabricating it into a resistive wearable sensor connected to a LED lamp (Figure 4a). The performance of the PHEA-TA@MXene organohydrogel as strain sensor was then investigated. The sensitivity was evaluated through gauge factor (GF), which was defined as the ratio of the relative resistance variation ($\Delta R/R_0$) to the applied strain (ϵ). As shown in Figure 4b, the GF value was 3.99 at below 400% strain and 7.79 at 400–700% strain, respectively, indicating the high sensitivity of the PHEA-TA@MXene organohydrogel sensor within a large sensing range. Under increasing increments of deformation (30, 40, 50, 60, 100, and 200% stretching), our gel strain sensor exhibited consistent and distinctly different response signals (Figure S23, Supporting Information), demonstrating its ability to differentiate different

levels of strains with good accuracy. Figure 4c shows that the resistance signals were almost the same when the organohydrogel was stretched repeatedly at 100% strain under different strain rates, indicating the detected signal output was independent of the stretching rate. Furthermore, 500 consecutive cycles under 50% strain were conducted to investigate the sensing stability. As shown in Figure 4d, the resistance change degree of the organohydrogel sensor was basically unchanged in each cycle, manifesting the high stability and durability. The slight fluctuation may be due to the small strain disturbance during the cyclic process. Such excellent strain-sensing performances may be attributed to the effective conductive path formed by MXene nanosheets and high resilience of the organohydrogel.^[58]

The excellent sensing performances and good self-adhesion make the organohydrogel an excellent candidate for wearable sensors to monitor human motions and physiological signals in real-time. When the wearable sensor was installed on the finger, the response signal exhibited a monotonic increase with the increase of the bending angles of finger from 0 to 30° , 60° , and 90° , and the response signal was almost constant during periodic bending of the finger at the same angle (Figure S24, Supporting Information). Figure 4e shows that the wearable sensor exhibited identical and stable response signal when the finger was bent slowly and when it was moved quickly, demonstrating its ability to detect signals of different frequencies. Similarly, other joint movements such as elbow, neck, and knee can also be accurately detected by the wearable sensor (Figure S25, Supporting Information). Particularly, even in harsh environments ($-40\text{ }^{\circ}\text{C}$), the wearable sensor could still detect the joint movements due to the anti-freezing nature of the organohydrogel (Figure S26, Supporting Information). Our wearable sensor can also detect complex facial expressions, including speaking, smiling, frowning, and chewing (Figure 4f; Figure S27, Supporting Information). When the same English word “Thank you” was repeated, the wearable sensor effectively exhibited sound recognition by detecting consistent and stable signals (Figure 4f). To further demonstrate its potential of participating in different types of sensors, the organohydrogel was assembled as skin electrode to detect pressure changes that correlate to electrophysiological signals, such as electrocardiogram (ECG) and electromyography (EMG). As shown in Figure 4g, to measure the ECG signals, two pieces of the organohydrogel were attached to the left and right arm, serving as working electrode and the reference electrode, respectively, and one organohydrogel piece was placed on the right calf as the grounding electrode. The ECG signals recorded with the organohydrogel electrode exhibited clear PQRST waveforms (Figure 4h), which were nearly the same as those recorded with commercial electrode (Figure 4i). Similar experiments were used to evaluate the EMG monitoring ability of the organohydrogel electrode (Figure S28, Supporting Information). The changes of biological potential caused by the switch between the relaxed and tense state of the flexor carpi were recorded. The organohydrogel electrode can monitor the steady EMG signals when the hand gripped different forces, which was comparable to the commercial electrode.

Aside from strain sensing, the PHEA-TA@MXene organohydrogel also had excellent thermal sensation owing to the thermal effect of MXene nanosheets.^[59,60] The resistance temperature coefficient (TCR) was used to evaluate the sensitivity of thermal

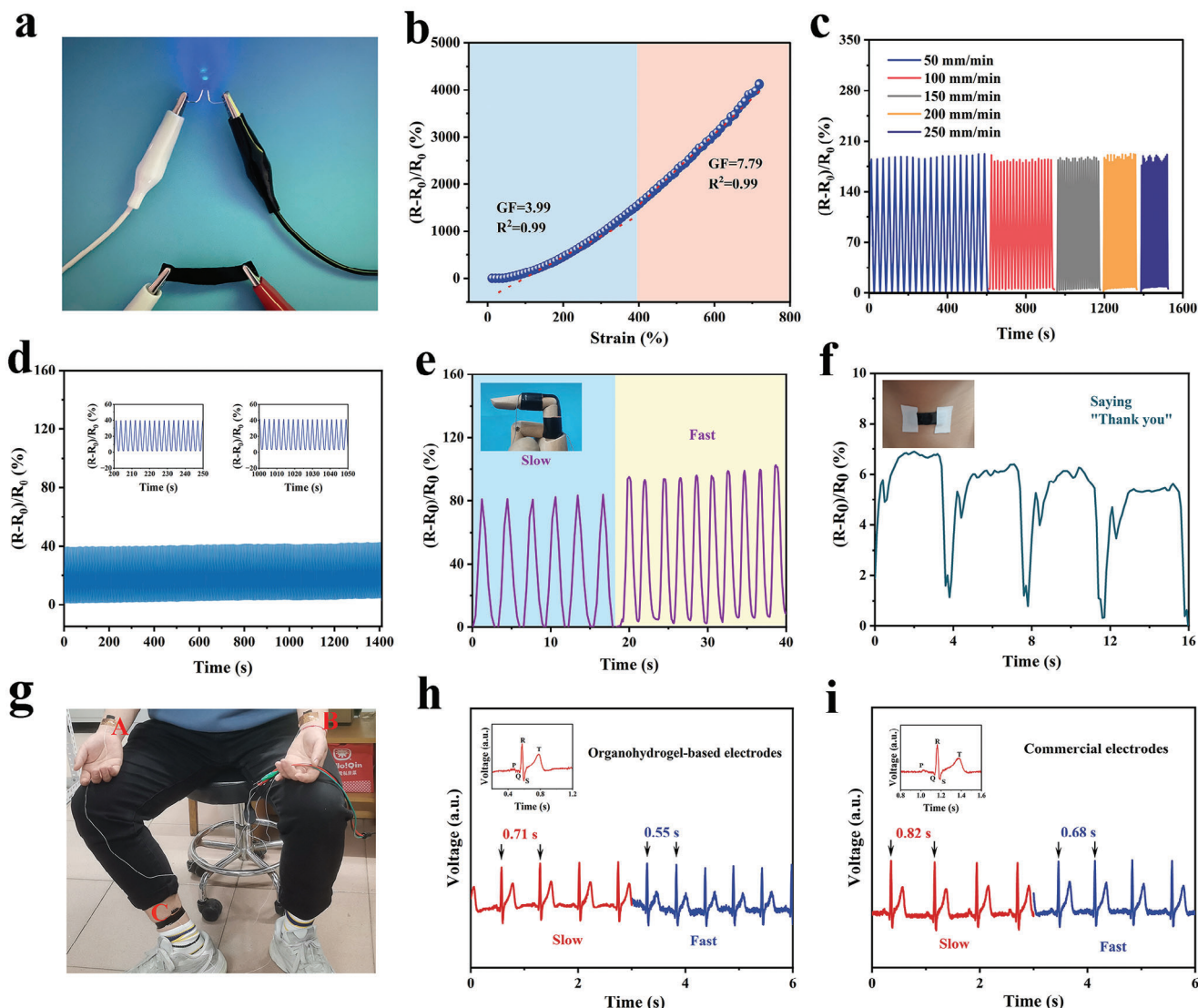


Figure 4. Strain sensing performance of the PHEA-TA@MXene organohydrogel and its application as wearable sensors. a) Photo showing the luminance of LED using the PHEA-TA@MXene organohydrogel as a conductor in series circuits. b) Relative resistance variation ($\Delta R/R_0$) of a PHEA-TA@MXene organohydrogel sensor as a function of strain and the corresponding GF. c) Relative resistance variation under cyclic stretching-releasing at different stretching rates (50, 100, 150, 200, and 250 mm min^{-1}) for 100% strain. d) Relative resistance variation under successive 500 loading-unloading cycles with a strain of 50%. The inset are 20 cycles of initial and final sections, respectively. Relative resistance changes of the PHEA-TA@MXene organohydrogel sensor in response to e) finger bending at different speeds and f) saying “Thank you”. g) Schematic diagram of the setup for the ECG detection. ECG monitoring with using h) PHEA-TA@MXene organohydrogel electrodes and i) commercial Ag/AgCl gel electrodes.

response, which is defined as $\text{TCR} = [(R_T - R_0)/R_0]/\Delta T$, where R_0 is the initial resistance at 20 °C and R_T is the instantaneous resistance at the measured temperature. As shown in **Figure 5a**, the relative resistance of the organohydrogel temperature sensor decreased significantly as the temperature rised from 20 to 80 °C. The obtained TCR was -2.65% and $-0.66\% \text{ } ^\circ\text{C}^{-1}$ in the 20–50 °C and 50–80 °C temperature ranges, respectively, which surpassed that of most previously reported temperature sensors.^[61–66] The great negative TCR behavior can be ascribed to the thermal-induced tunneling effect.^[67] The MXenes with surface functional groups (–F and –OH) exhibits narrow bandgap semiconducting properties.^[68] Based on the narrow bandgap semiconductive behavior, the thermal disturbance caused by the increased temper-

ature endows electrons with sufficient energy to achieve transitions as well as boost carrier concentration. As a result, the conductivity of MXene can be enhanced with the increasing temperature, promoting the electron transmission efficiency. Consequently, the PHEA-TA@MXene organohydrogel exhibits excellent temperature sensing performances. In order to explore the organohydrogel’s resistance changes in response to temperature changes, a sample was placed in hot water, then in ice water, for multiple cycles to simulate rapid temperature changes. The current signal of the temperature sensor changed rapidly after being exposed to a heat source (50 °C) or a cold source (0 °C), which can be completely recovered after removing heat or cool sources (Figure S29a,b, Supporting Information). As shown in

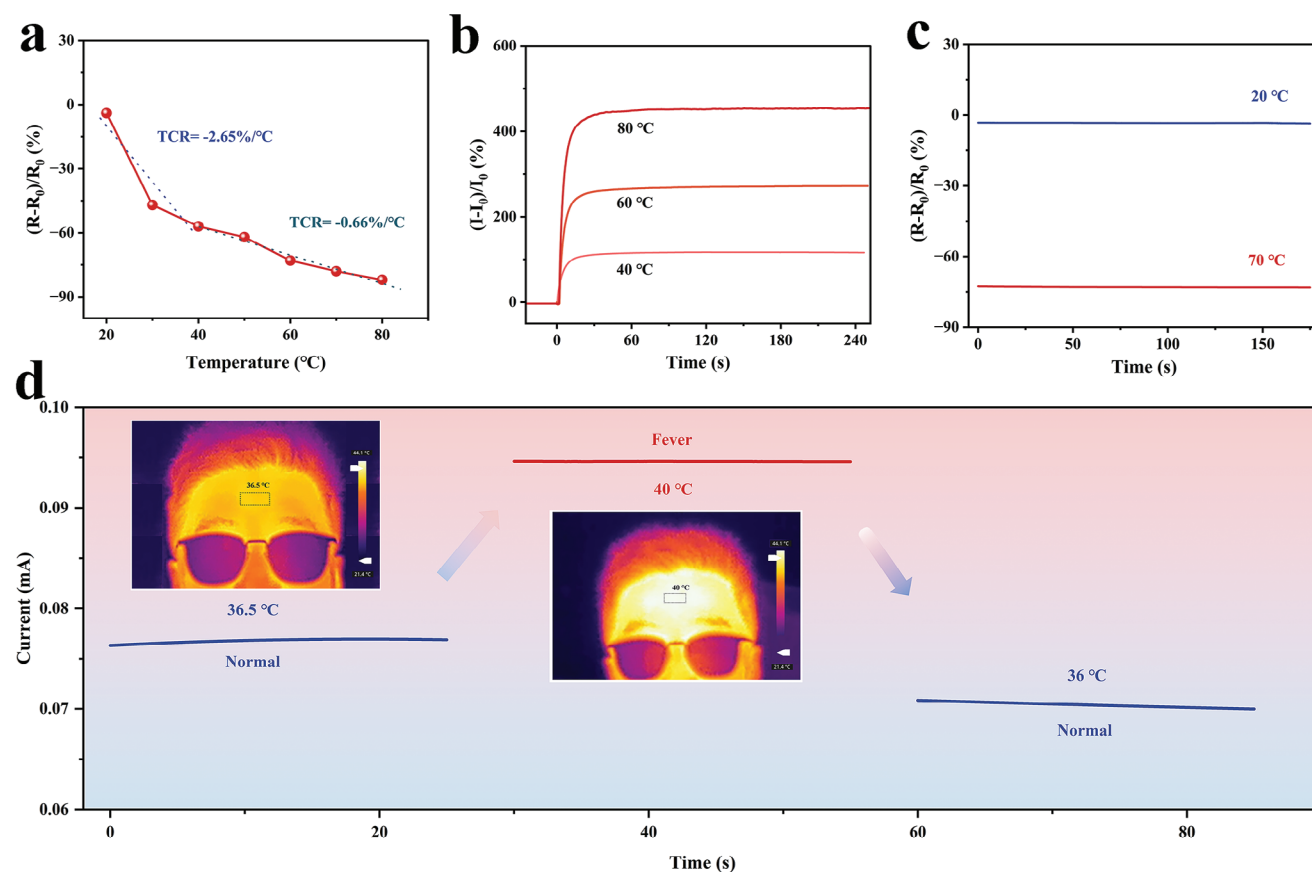


Figure 5. Temperature-sensing performances and application of the PHEA-TA@MXene organohydrogel. a) Relative resistance changes of the PHEA-TA@MXene organohydrogel upon increasing temperature from room temperature 20 to 80 °C. b) Current variation of the PHEA-TA@MXene organohydrogel responding to heat sources of different temperatures (40, 60, and 80 °C). c) Relative resistance changes of the PHEA-TA@MXene organohydrogel as a function of time at 20 and 70 °C. d) Current variation of PHEA-TA@MXene organohydrogel before and after the “artificial fever” (Inset: Infrared thermal images of the human forehead before and after the “artificial fever”).

Figure 5b, when the temperature sensor was exposed to different temperatures (40, 60, and 80 °C), the current signal quickly plateaued. These results demonstrate that the organohydrogel temperature can rapidly respond to temperature with excellent recoverability. The organohydrogel temperature sensor also had excellent stability, as can be seen from the very small resistance deviation at each temperature (20 and 70 °C) in Figure 5c. The organohydrogel temperature sensor was further utilized as wearable sensor for human temperature monitoring. A heat source was used to change the temperature of the sensor by approaching/moving away from the human forehead, and an infrared (IR) thermography camera was applied to instantaneously detect the temperature. As shown in the Figure 5d, the sensor displayed a current of 0.076 mA corresponding to the normal temperature of the human body (36.5 °C). In contrast, the current sharply rose to 0.095 mA when the human body temperature increased to 40 °C. Due to the excellent thermal sensitivity of the organohydrogel, apparent current changes could be observed within narrow temperature range. It is worth noting that this “fever signal” based on accurate and repeatable current indications could also be used to reflect the process of fever relief. Therefore, the temperature response of the organohydrogel sensor could be used in place of a thermometer to monitor patients with fever. The

systematic comparison of the performance parameters and applications of our PHEA-TA@MXene organohydrogel with previously reported conductive fillers-composited gels was shown in Table S1 (Supporting Information). It can be seen that the organohydrogel exhibited highly desirable overall performances including high stretchability, low hysteresis, adhesiveness and excellent freezing tolerance compared with other conductive fillers-composited gels. In addition, our organohydrogel-based wearable sensors had the better combination of high-performance multi-sensing capability including high strain sensitivity in wide strain range for accurate of various detection of human motions and electrocardiogram signals, and high thermosensitive capacities for body temperature monitoring.

2.7. Generalizability of TA@MXene Nano-Motif for Constructing High-Strength MXene- Composited Gels with High Resilience

The construction of stable, high-strength and highly elastic MXene-composited gels relies on the high stability of TA@MXene in aqueous dispersion, and the high-density hydrogen bonds between the polymer network and the polyhydroxyl groups on TA@MXene surface. Therefore, the TA@MXene

nano-motif can be also incorporated into other gel networks with abundant hydrogen bond donor or acceptor to prepare stable MXene-based gels with improved mechanical properties and high resilience. As a demo, the TA@MXene nano-motif was introduced into polyacrylic acid (PAA) and polyacrylamide (PAM) organohydrogel networks, respectively. Compared to PAM organohydrogel with a tensile stress of 41.6 kPa and a tensile strain of 628.1%, the PAM-TA@MXene organohydrogel had a higher tensile stress of 115.4 kPa and tensile strain of 781.6% (Figure S30a, Supporting Information). Likewise, the constructed PAA-TA@MXene organohydrogel demonstrated significantly better mechanical properties than that of PAA organohydrogel (Figure S30b, Supporting Information). The tensile strength and strain of the PAA-TA@MXene organohydrogel reached to 218.8 kPa and 948.3%, which were 2.05 and 1.35 times of that of the PAA organohydrogel, respectively. Moreover, ten successive cyclic tensile experiments at 300% show that both of PAM-TA@MXene and PAA-TA@MXene organohydrogels had smaller residual strains than that of PAM and PAA organohydrogels, respectively (Figure S31, Supporting Information), demonstrating the higher resilience. Therefore, based on stable TA@MXene nano-motif, various gels could be appropriately selected to prepare high-strength MXene-based gels with functionality, expanding their applications in advanced electronic devices.

3. Conclusion

In conclusion, we have proposed a facile strategy to inhibit the oxidation of MXene in water environment by encapsulating MXene nanosheets with TA molecules, obtaining a highly stable TA@MXene nano-motif in aqueous dispersion. By incorporating this TA@MXene into physically crosslinked PHEA network in Gly/water binary solvent, a conductive organohydrogel with comprehensive performances including high stretchability, low hysteresis, self-adhesion, and environmental stability was successfully synthesized. Thanks to the unique energy dissipation mechanism originated from the high-density hydrogen bonding between PHEA chains and TA@MXene, the organohydrogel exhibited large stretchability (>500%) with low hysteresis (<3%) and excellent fatigue resistance. Moreover, owing to the formation of Gly/water binary solvent system, the organohydrogel showed excellent freezing resistance (-40°C) and moisturizing retention properties (>7 days), ensuring the stable performance in long-term use and under extreme conditions. The organohydrogel was also highly adhesive due to the presence of catechol groups. Benefiting from all these performances, the organohydrogel-based sensor demonstrated high strain sensitivity with large working range over wide temperatures, highly reliability and durability, and high thermosensitive capacities. As a result, the wearable sensor can be used to accurately detect human motions in different modes and electrocardiogram signals with high repeating stability, as well as body temperature. The TA@MXene nano-motif constructed in this work can be introduced into various network structure to fabricate high-performance and stable MXene-based soft gels as promising materials for intelligent sensing applications.

4. Experimental Section

Materials: Ti_3AlC_2 powder was purchased from 11 technology Co., Ltd. Gly (AR, 99%), 2-hydroxyethyl acrylate (HEA), acrylamide (AM), acrylic acid (AA), ammonium persulfate (APS), tannic acid (TA), hydrochloric acid (HCl), lithium fluoride (LiF), and tris-HCl buffer were provided by Aladdin Bio Chemical Technology Co., Ltd. All chemicals were used without further purification.

Fabrication of MXene Nanosheets: Ti_3C_2 MXene was synthesized by etching Al layer from the MAX phase according to the previous reports.^[39,40] To be specific, 1 g Ti_3AlC_2 was added into 20 mL HCl (9 M) and LiF (1.6 g) aqueous solution and the resulting mixture was magnetically stirred at 35°C for 36 h. Afterward, the suspension liquid was washed with deionized water and centrifuged at 3500 rpm until the supernatant closed to the neutral. The obtained precipitant was redispersed in deionized water and sonicated for 1.5 h in an ice bath with Ar bubbling. After another centrifugation for 1 h at 3500 rpm, Ti_3C_2 MXene dispersion with a dark color was gathered. Finally, the supernatant was freeze-dried to obtain MXene nanosheets.

Preparation of TA@MXene Dispersions: A certain amount of MXene nanosheets was taken in deionized water and dispersed by ultrasound for 30 min. Then, the same mass of TA was added to the above solution and the pH value of the solution was regulated to 8 by dropping tris buffer, followed by magnetic stirring for 12 h to obtain the dark green TA@MXene dispersion.

Synthesis of the PHEA-TA@MXene Organohydrogel: The PHEA-TA@MXene organohydrogel was prepared by one-pot method. First, a certain amount of Gly was added to the TA@MXene dispersion under magnetic stirring for 10 min to form a uniform TA@MXene Gly/ H_2O binary dispersion system. Then, HEA was added and magnetically stirred for 20 min under Ar flow. After adding APS (0.5%), the mixed solution was injected into the mold and placed in the oven at 60°C for 4 h to form the PHEA-TA@MXene organohydrogel. The various gel samples of different weight ratios of TA@MXene, Gly and HEA were prepared followed by same procedure.

General Characterization: The morphology of MXene and TA@MXene nanosheets and the microstructure of the organohydrogel were observed by scanning electron microscope (SEM, S-4800II) and transmission electron microscope (TEM, HT7700). Atomic force microscope (AFM, Multi-mode 8) was used to further observe the geometric morphology of MXene nanosheets. The X-ray diffraction (XRD) patterns of MXene nanosheets and gels were obtained by Siemens D5000 X-ray diffractometer (Cu $K\alpha$, $\lambda = 1.5418 \text{ \AA}$) on a Rigaku Miniflex apparatus. Fourier transform infrared (FTIR) spectroscopy was used to determine the chemical composition of the prepared gels in the range of $400 - 4000 \text{ cm}^{-1}$. X-ray photoelectron spectroscopy (XPS, Thermo Scientific Escalab 250Xi+) was used to observe the oxidation degree of MXene and TA@MXene nanosheets.

Supporting Information

Supporting Information is available from the Wiley Online Library or from the author.

Acknowledgements

The authors greatly appreciate the financial support of the National Natural Science Foundation of China (Nos. 22102139 and 22072127), the Hebei Natural Science Foundation (Nos. B2021203001 and B2021203016), the Science and Technology Project of Hebei Education Department (No. ZD2022147), and the Special Project for Local Science and Technology Development Guided by the Central Government of China (Nos. 216Z1301G and 226Z1401G).

Conflict of Interest

The authors declare no conflict of interest.

Data Availability Statement

The data that support the findings of this study are available from the corresponding author upon reasonable request.

Keywords

high stability, low hysteresis, MXene nanosheets, organohydrogels, wearable sensors

Received: December 11, 2023

Revised: February 17, 2024

Published online:

- [1] L. Xu, Z. Huang, Z. Deng, Z. Du, T. L. Sun, Z. H. Guo, K. Yue, *Adv. Mater.* **2021**, *33*, 2105306.
- [2] Y. Niu, H. Liu, R. He, M. Luo, M. Shu, F. Xu, *Small* **2021**, *17*, 2101151.
- [3] X. Sun, F. Yao, J. Li, *J. Mater. Chem. A* **2020**, *8*, 18605.
- [4] X. Shen, Q. Zheng, K. J. K. Prog, *Mater. Sci.* **2021**, *115*, 100708.
- [5] Q. Yu, Z. Qin, F. Ji, S. Chen, S. Luo, M. Yao, X. Wu, W. Liu, X. Sun, H. Zhang, Y. Zhao, F. Yao, J. Li, *Chem. Eng. J.* **2021**, *404*, 126559.
- [6] G. Ge, W. Yuan, W. Zhao, Y. Lu, Y. Zhang, W. Wang, P. Chen, W. Huang, W. Si, X. Dong, *J. Mater. Chem. A* **2019**, *7*, 5949.
- [7] Y. Zhu, J. Liu, T. Guo, J. J. Wang, X. Tang, V. Nicolosi, *ACS Nano* **2021**, *15*, 1465.
- [8] K. Li, J. Zhao, A. Zhussupbekova, C. E. Shuck, L. Hughes, Y. Dong, S. Barwich, S. Vaesen, I. V. Shvets, M. Mobius, W. Schmitt, Y. Gogotsi, V. Nicolosi, *Nat. Commun.* **2022**, *13*, 6884.
- [9] A. Vahidmohammadi, M. Mojtavavi, N. M. Caffrey, M. Wanunu, M. Beidaghi, *Adv. Mater.* **2019**, *31*, 1806931.
- [10] C. Zhang, L. Mckee, M. P. Kremer, S. H. Park, O. Ronan, A. Seral-Ascaso, S. Barwich, C. O. Coileain, N. Mcevoy, H. C. Nerl, B. Anasori, J. N. Coleman, Y. Gogotsi, V. Nicolosi, *Nat. Commun.* **2019**, *10*, 1795.
- [11] M. Han, C. E. Shuck, R. Rakhmanov, D. Parchment, B. Anasori, C. M. Koo, G. Friedman, Y. Gogotsi, *ACS Nano* **2020**, *14*, 5008.
- [12] V. Kamysbayev, A. S. Filatov, H. Hu, X. Rui, F. Lagunas, D. Wang, R. F. Klie, D. V. Talapin, *Science* **2020**, *369*, 979.
- [13] Y. F. Zhang, Z. S. Xu, Y. Yuan, C. Y. Liu, M. Zhang, L. Q. Zhang, P. B. Wan, *Adv. Funct. Mater.* **2023**, *33*, 2300299.
- [14] H. Liao, X. Guo, P. Wan, G. Yu, *Adv. Funct. Mater.* **2019**, *29*, 1904507.
- [15] Y. B. Feng, H. Liu, W. H. Zhu, L. Guan, X. T. Yang, A. V. Zvyagin, Y. Zhao, C. Shen, B. Yang, Q. Lin, *Adv. Funct. Mater.* **2021**, *31*, 2105264.
- [16] J. Liu, C. Xie, A. Kretzschmann, K. Koynov, H. J. Butt, S. Wu, *Adv. Mater.* **2020**, *32*, 1908324.
- [17] P. He, J. Wu, X. Pan, L. Chen, K. Liu, H. Gao, H. Wu, S. Cao, L. Huang, Y. Ni, *J. Mater. Chem. A* **2020**, *8*, 3109.
- [18] J. Liu, Z. Chen, Y. Chen, H. U. Rehman, Y. Guo, H. Li, H. Liu, *Adv. Funct. Mater.* **2021**, *31*, 2101464.
- [19] H. Zhou, J. Lai, X. Jin, H. Liu, X. Li, W. Chen, A. Ma, X. Zhou, *Chem. Eng. J.* **2021**, *413*, 127544.
- [20] Y. Ye, Y. Zhang, Y. Chen, X. Han, F. Jiang, *Adv. Funct. Mater.* **2020**, *30*, 2003430.
- [21] J. Wang, F. Tang, C. Yao, L. Li, *Adv. Funct. Mater.* **2023**, *33*, 2214935.
- [22] B. Huang, Z. Zhou, L. Wei, Q. Song, W. Yu, Y. Zhou, R. Hu, W. Zhang, C. Lu, *Composites, Part B* **2021**, *225*, 109261.
- [23] X. Su, S. Mahalingam, M. Edirisinghe, B. Chen, *ACS Appl. Mater. Interfaces* **2017**, *9*, 22223.
- [24] M. Zhu, Y. Liu, B. Sun, W. Zhang, X. Liu, H. Yu, Y. Zhang, D. Kuckling, H. J. P. Adler, *Macromol. Rapid. Commun.* **2006**, *27*, 1023.
- [25] F. Shahzad, M. Alhabeab, C. B. Hatter, B. Anasori, S. M. Hong, C. M. Koo, Y. Gogotsi, *Science* **2016**, *353*, 1137.
- [26] Y. Li, R. Z. Fu, Z. G. Duan, C. H. Zhu, D. Fan, *ACS Nano* **2022**, *16*, 7502.
- [27] J. Kim, Y. Yoon, S. K. Kim, S. Park, W. Song, S. Myung, H. K. Jung, S. S. Lee, D. H. Yoon, K. S. An, *Adv. Funct. Mater.* **2021**, *31*, 2008722.
- [28] T. Habib, X. Zhao, S. A. Shah, Y. Chen, W. Sun, H. An, J. L. Lutkenhaus, M. Radovic, M. J. Green, *npj 2D Mater. Appl.* **2019**, *3*, 8.
- [29] Y. J. Wan, K. Rajavel, X. M. Li, X. Y. Wang, S. Y. Liao, Z. Q. Lin, P. L. Zhu, R. Sun, C. P. Wong, *Chem. Eng. J.* **2021**, *408*, 127303.
- [30] M. C. Kreckler, D. Bukharina, C. B. Hatter, Y. Gogotsi, V. V. Tsukruk, *Adv. Funct. Mater.* **2020**, *30*, 2004554.
- [31] X. Zhao, A. Vashisth, E. Pehrn, W. Sun, S. A. Shah, T. Habib, Y. Chen, Z. Tan, J. L. Lutkenhaus, M. Radovic, M. J. Green, *Matter* **2019**, *1*, 513.
- [32] X. Yang, Y. Yao, Q. Wang, K. Zhu, K. Ye, G. Wang, D. Cao, J. Yan, *Adv. Funct. Mater.* **2021**, *32*, 2109479.
- [33] Y. Wei, L. Xiang, H. Ou, F. Li, Y. Zhang, Y. Qian, L. Hao, J. Diao, M. Zhang, P. Zhu, Y. Liu, Y. Kuang, G. Chen, *Adv. Funct. Mater.* **2020**, *30*, 2005135.
- [34] Y. Z. Zhang, K. H. Lee, D. H. Anjum, R. Sougrat, Q. Jiang, H. Kim, H. N. Alshareef, *Sci. Adv.* **2018**, *4*, aat0098.
- [35] A. Chae, G. Murali, S.-Y. Lee, J. Gwak, S. J. Kim, Y. J. Jeong, H. Kang, S. Park, A. S. Lee, D.-Y. Koh, I. In, S.-J. Park, *Adv. Funct. Mater.* **2023**, *33*, 2213382.
- [36] N. Wu, Z. Zeng, N. Kummer, D. Han, R. Zenobi, G. Nyström, *Small Methods* **2021**, *5*, 2100889.
- [37] J. Yan, C. E. Ren, K. Maleski, C. B. Hatter, B. Anasori, P. Urbankowski, A. Sarycheva, Y. Gogotsi, *Adv. Funct. Mater.* **2017**, *27*, 1701264.
- [38] M. Wan, S. Song, X. Jiang, Z. Liu, Y. Luo, X. Gao, J. Liu, J. Shen, *ACS Appl. Nano Mater.* **2022**, *5*, 15583.
- [39] S. Song, X. Jiang, H. Shen, W. Wu, Q. Shi, M. Wan, J. Zhang, H. Mo, J. Shen, *ACS Appl. Bio Mater.* **2021**, *4*, 6912.
- [40] I. Persson, J. Halim, T. W. Hansen, J. B. Wagner, V. Darakchieva, J. Palisaitis, J. Rosen, P. O. A. Persson, *Adv. Funct. Mater.* **2020**, *30*, 1909005.
- [41] X. Wang, X. Wang, J. Yin, N. Li, Z. Zhang, Y. Xu, L. Zhang, Z. Qin, T. Jiao, *Composites, Part B* **2022**, *241*, 110052.
- [42] X. Wang, N. Li, J. Yin, X. Wang, L. Xu, T. Jiao, Z. Qin, *Sci. China Mater.* **2022**, *66*, 272.
- [43] Y. Yu, P. Yi, W. Xu, X. Sun, G. Deng, X. Liu, J. Shui, R. Yu, *Nano-Micro Lett.* **2022**, *14*, 77.
- [44] B. Ying, R. Z. Chen, R. Zuo, J. Li, X. Liu, *Adv. Funct. Mater.* **2021**, *31*, 2104665.
- [45] X. Li, L. He, Y. Li, M. Chao, M. Li, P. Wan, L. Zhang, *ACS Nano* **2021**, *15*, 12453.
- [46] J. Huang, X. Huang, P. Wu, *Chem. Eng. J.* **2022**, *428*, 132515.
- [47] T. N. Lam, G. S. Lee, B. Kim, *Compos. Sci. Technol.* **2021**, *210*, 108811.
- [48] N. Tang, C. Zhou, D. Qu, *Small* **2020**, *16*, 2001363.
- [49] J. Ryu, J. Kim, J. Oh, *Nano Energy* **2019**, *55*, 348.
- [50] G. Shen, B. Chen, T. Liang, *Adv. Electron. Mater.* **2020**, *6*, 1901360.
- [51] A. Chen, J. Zhang, J. Zhu, *J. Mater. Chem. A* **2023**, *11*, 4977.
- [52] G. Xue, Y. Shi, S. Wang, *Chem. Eng. J.* **2023**, *456*, 140976.
- [53] Y. Li, P. Yu, J. Wen, H. Sun, D. Wang, J. Liu, J. Li, H. Chu, *Adv. Funct. Mater.* **2022**, *32*, 2110720.
- [54] H. Zhao, S. Hao, Q. Fu, X. Zhang, L. Meng, F. Xu, J. Yang, *Chem. Mater.* **2022**, *34*, 5258.
- [55] M. Soni, M. Bhattacharjee, M. Ntagios, R. Dahiya, *IEEE Sens. J.* **2020**, *20*, 7525.
- [56] Z. H. Qin, D. Y. Dong, M. M. Yao, Q. Y. Yu, X. Sun, Q. Guo, H. T. Zhang, F. L. Yao, J. J. Li, *ACS Appl. Mater. Interfaces* **2019**, *11*, 21193.
- [57] X. Li, L. He, Y. Li, M. Chao, M. Li, P. Wan, L. Zhang, *ACS Nano* **2021**, *15*, 7765.
- [58] J. Yu, Y. Feng, D. Sun, W. Ren, C. Shao, R. Sun, *ACS Appl. Mater. Interfaces* **2022**, *14*, 10886.
- [59] X. Zhou, A. Rajeev, A. Subramanian, Y. Li, N. Rossetti, G. Natale, G. A. Lodygensky, F. Cicoira, *Acta Biomater.* **2022**, *145*, 436.

- [60] D. Xu, Z. Li, L. Li, J. Wang, *Adv. Funct. Mater.* **2020**, *30*, 2000712.
- [61] W. Honda, S. Harada, S. Ishida, T. Arie, S. Akita, K. Takei, *Adv. Mater.* **2015**, *27*, 4674.
- [62] T. Q. Trung, S. Ramasundaram, B. U. Hwang, N. E. Lee, *Adv. Mater.* **2016**, *28*, 502.
- [63] G. Ge, Y. Lu, X. Qu, W. Zhao, Y. Ren, W. Wang, Q. Wang, W. Huang, X. Dong, *ACS Nano* **2020**, *14*, 218.
- [64] B. W. An, S. Heo, F. B. Ji, J. U. Park, *Nat. Commun.* **2018**, *9*, 2458.
- [65] A. Chhetry, S. Sharma, S. C. Barman, H. Yoon, S. Ko, C. Park, J. Y. Park, *Adv. Funct. Mater.* **2021**, *31*, 2007661.
- [66] J. Wu, W. Huang, Y. Liang, Z. Wu, B. Zhong, Z. Zhou, X. Xie, *Adv. Electron. Mater.* **2021**, *7*, 2001084.
- [67] H. Liu, C. Du, L. Liao, H. Zhang, H. Zhou, W. Zhou, W. Huang, *Nat. Commun.* **2022**, *13*, 3420.
- [68] S. Zheng, H. Wang, P. Das, Y. Zhang, Y. Cao, J. Ma, S. F. Liu, Z.-S. Wu, *Adv. Mater.* **2021**, *33*, 2005449.